JPE 19-1-2

https://doi.org/10.6113/JPE.2019.19.1.11
ISSN(Print): 1598-2092 / ISSN(Online): 2093-4718

New ZVZCT Bidirectional DC-DC Converter Using Coupled Inductors

Wei Qian*, Xi Zhang†, Zhe Li*, Wenqiang Jin*,**, and Jochen Wiedemann***

†,*School of Mechanical and Power Engineering, Shanghai Jiao Tong University, Shanghai, China
**Argonne National Lab, Lemont, IL, USA
***Department of Automotive Engineering, University of Stuttgart, Stuttgart, Germany

Abstract

In this study, a novel zero voltage zero current transition (ZVZCT) bidirectional DC-DC converter is proposed by employing coupled inductors. This converter can turn the main switch on at ZVZCT and it can turn it off with zero voltage switching (ZVS) for both the boost and buck modes. These characteristics are obtained by using a simple auxiliary sub-circuit regardless of the power flow direction. In the boost mode, the auxiliary switch achieves zero current switching (ZCS) turn-on and ZVS turn off. Due to the coupling inductors, this converter can make further efficiency improvements because the resonant energy in the capacitor or inductor can be transferred to the load. The main diode operates with ZVT turn-on and ZCS turn-off in the boost mode. For the buck mode, there is a releasing circuit to conduct the currents generated by the magnetic flux leakage to the output. The auxiliary switch turns on with ZCS and it turns off with ZVT. The main diode also turns on with ZVT and turns off with ZCS. The design method and operation principles of the converter are discussed. A 500 W experimental prototype has been built and verified by experimental results.

Key words: Bidirectional, Coupled inductor, DC-DC converter, ZVZCT

I. INTRODUCTION

Recently, the research on bidirectional DC-DC converters (BDCs) has become an important topic due to its application in energy recovery and energy storage systems. DC-DC converters are widely applied as such in solar power supplies, electric vehicles, energy storage systems, fuel cell vehicles, etc. [1]-[6]. BDCs can keep storage devices healthy by controlling the discharge and charge [8]. Bi-directional converters have two types: isolated and non-isolated. BDCs are widely applied due to their simple structure and control. A high switching frequency is a good solution to achieve a high-power density in BDCs. Obviously, hard switching (HS) limits the switching frequency, and increases both the electromagnetic interference (EMI) and switching loss. To solve these problems, soft-switching has been developed in BDCs. The task is the challenging since soft switching must be ensured for the both power flow directions. Studies for soft switching have yielded different topologies, and they can be classified into three basic types.

1) The first type of solution adopts the interleaved topology [7]. In some DC-DC converters, parallel connections are used to form interleaved structures. To realizing soft switching, the charge and discharge of the bypass capacitors of the switches can be buffered by the positive and negative flowing of the inductance current. However, too many components, such as double switches and double main inductors, can result in the power density becoming lower, which makes the control algorithm more complex.

2) The second type of solution is to produce an oscillation between the inductors and capacitors, [9]-[12], which makes it possible for zero voltage or zero current to be obtained. In [13], the auxiliary switch is operated two times in one cycle, which increases the complex of the control method. In [14], the circulating current of the auxiliary switchings are reduced by the conduction time reduction. However, when the auxiliary switch turns off, the oscillation between the inductors and

Manuscript received May 9, 2018; accepted Sep. 15, 2018
Recommended for publication by Associate Editor Jongbok Baek.
†Corresponding Author: braver1980@sjtu.edu.cn
Tel: +86-13918913376, Shanghai Jiao Tong University
*Sch. of Mechanical and Power Eng., Shanghai Jiao Tong Univ., China
**Argonne National Lab, USA
***Dept. of Automotive Engineering, University of Stuttgart, Germany

snubber capacitors in series results in an undesirable oscillation, which reduces the converter efficiency and increases the voltage stress of the semiconductor elements. In [15], a complicated soft-switching structure is applied to a converter. However, this has relative drawbacks. In [16], a converter is designed with an auxiliary switch operating twice in a switching period. As a result, the switching loss increases, the control strategy becomes more complex, and the switching frequency is limited. In addition, the main switch suffers from high current stress.

In [17], the bi-directional DC-DC converter has the advantage of fewer components, a simple structure and a simple control method. The boost and buck modes share the same resonant circuits. Therefore, the efficiency is high. However, the resonant inductance used to realize ZVS is located in the main circuit of the topology. Thus, the soft switching characteristics of the topology are affected more by the operating state and load of the main circuit. On the other hand, it leads to instability of the main circuit voltage.

3) The third type of solution uses coupled inductors to provide soft-switching of the auxiliary switches [18]-[24]. The coupled inductor is used as a resonant inductor, and all of the magnetic elements are made on a single magnetic core. Therefore, the converter weight and volume are reduced. However, in some converters, the voltage stress of the auxiliary switch exceeds the high voltage side.

In [25], the authors presented a family of snubber active structures using feedback inductors. Although there are more diodes, the feedback inductance is used to transfer the resonant current to the load side to improve efficiency. However, the coupling factor of the feedback inductor is close to 1. Therefore, the topology cannot control the auxiliary switch current stress or reverse recovery current by designing the coupling coefficient.

In this study, a new ZVZCT bidirectional converter using coupled inductors is introduced. For the proposed converter, the soft switch can be implemented for all of the semiconductor components in the entire duty cycle range, regardless of the power flow direction. For this converter, the main switch is easy to control and does not have extra voltage or current stress. In the boost mode, the main switch turns on with ZVZCT and turns off with ZVS. The auxiliary switch turns on with ZCS and turns off at ZVS. In the buck mode, the main switch can be operated with ZVZCT turn-on and ZVS turn-off, and the auxiliary switch can also realize ZCS turn-on and ZVT turn-off.

For this topology, full coupling of the inductors is not necessary. Because the new topology is able to conduct leakage current through the energy release loop, the parasitic oscillation and current rush are eliminated. The coupling inductance is able to deliver resonant power to the output terminal through the coupling effect, and the current stress of the auxiliary switch can be limited, which reduces the conduction loss and improves the efficiency.

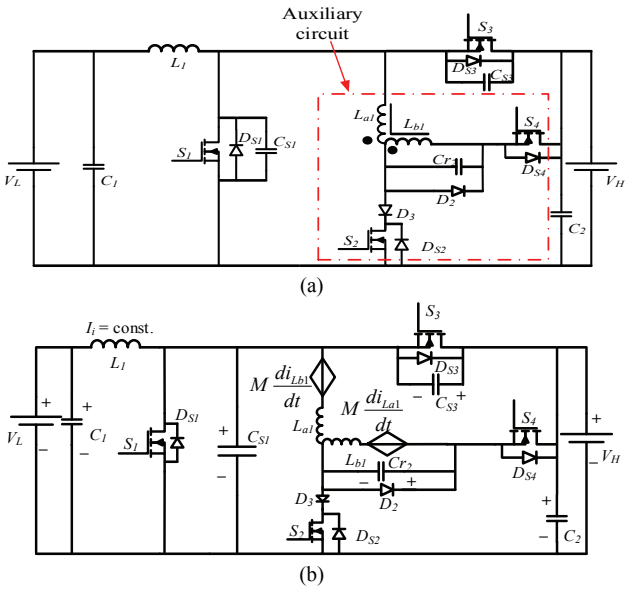

Fig. 1. The proposed DC/DC converter: (a) Proposed topology; (b) Equivalent circuit.

In the boost mode, extra resonance energy is transferred to the load side via the coupled inductor. Therefore, the current stress on the auxiliary switch is controllable. When designing the topology, the freewheeling current can be reduced by adjusting the coupling coefficient. As a result, the design flexibility of the topology is improved. On the other hand, when the auxiliary switch is off, the turn-off current and voltage are low. There is no current or voltage spike, which improves the working conditions of the auxiliary switch. With the same components, the load range for ZVZCT realization is expanded.

The rest of this paper is organized as follows. The second section describes the topology and working principle. The third section provides a parameter analysis and the topology design. In the fourth part, experimental results are discussed. The final section gives some conclusions.

II. Topology and Working Principle

The proposed ZVZCT bidirectional DC-DC converter is shown in Fig. 1(a), and Fig. 1(b) shows an equivalent circuit of this topology. The resonance part includes one resonant capacitor, a coupled-inductor, two diodes and two auxiliary switches, where v_{L1}, v_{La1} and v_{Lb1} are the voltages of the inductors; L_1, L_{a1} and L_{b1} are the inductances; M is the mutual inductance of L_{a1} and L_{b1}; and i_{L1}, i_{La1} and i_{Lb1} are the currents of L_1, L_{a1} and L_{b1}.

A. Boost Working Mode

In the boost mode, seven working modes are analyzed in one period. Fig. 2(a) shows each operation mode for the topology. Key waveforms of the boost mode are shown in Fig. 2(b).

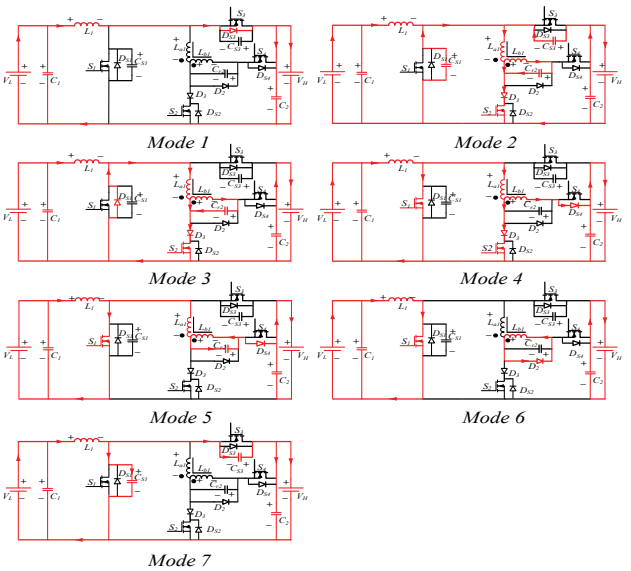

(a)

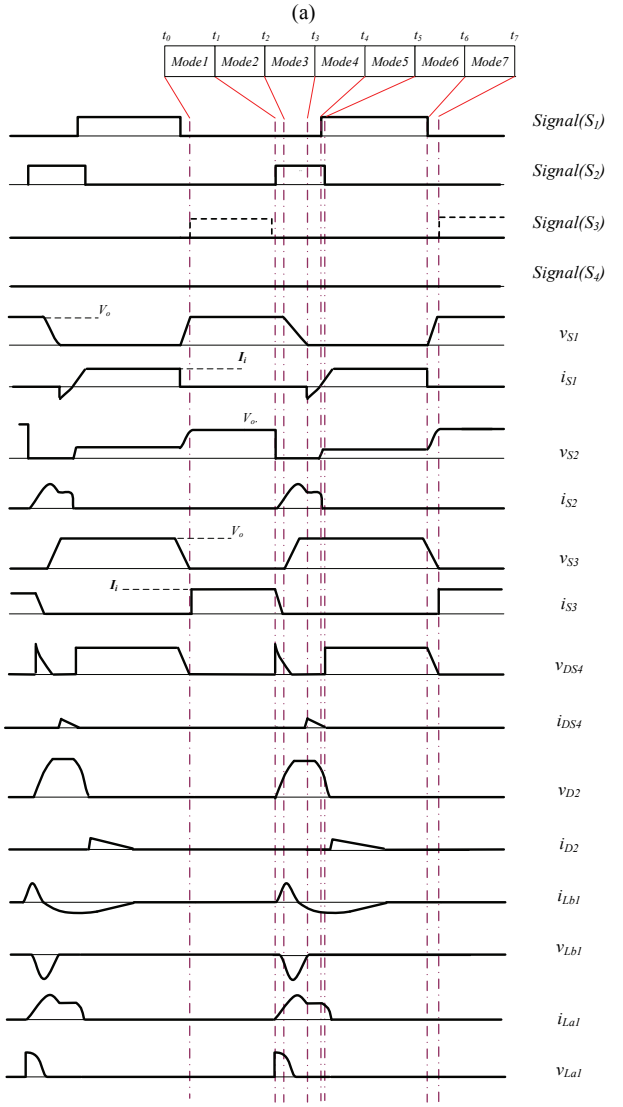

(b)

Fig. 2. Operations and principles for the boost mode: (a) Operation stages for the boost mode; (b) Key waveforms for the boost mode.

1) Mode 1 ($t_0 \le t < t_1$):

This is the main switch off mode for the traditional boost converter. In this interval, both S_1 and S_2 are off and D_{S3} is on. V_{S1} is equal to the output voltage. Therefore, there is no voltage stress on it. The converter energy is transfered from the low side to the high side.

2) Mode 2 ($t_1 \le t < t_2$):

The initial conditions at t_1 are $v_{CS1}=V_H$, $v_{Cr2}=0$, $i_{S1}=0$, $i_{S2}=0$, $i_{DS3}=I_i$ and $i_{La1}=i_{Lb1}=0$. The turn-on signal is implemented to S_2, and the resonance begins with L_{a1}, L_{b1}, C_{S1} and C_{S3}. This resonance provides S_2 with ZCS turn-on. Meanwhile, the current i_{CS3} falls down, and C_{r2} is charged. At the end of this mode, the resonance reduces the current of C_{S3} to zero. Therefore, S_3 achieves ZCS turn-off, and the capacitor C_{r2} voltage rises. The following equations are obtained in this mode by KVL:

$$\begin{cases} C_{s3}\dfrac{dv_{Cs3}}{dt} = i_{Cs3} \\ C_{s1}\dfrac{dv_{Cs1}}{dt} = i_{Cs1} \\ C_{r2}\dfrac{dv_{Cr2}}{dt} = i_{Cr2} \\ -M\dfrac{di_{Lb1}}{dt} + L_{a1}\dfrac{di_{La1}}{dt} + v_{Cs1} = 0 \\ -M\dfrac{di_{La1}}{dt} + L_{b1}\dfrac{di_{Lb1}}{dt} + v_{Cr2} = 0 \\ v_{Cs1} + v_{Cs3} = V_H \end{cases} \tag{1}$$

3) Mode 3 ($t_2 \le t < t_3$):

In mode 3, C_{S1} and C_{S3} have been discharged to zero and separately charged to the output voltage. Thus, S_3 does not suffer from voltage stress. D_{S1} is at the turn-on stage, and C_{r2} continues the charge. L_{a1}, L_{b1} and C_{r2} resonate though the body diode of S_1. Once C_{r2} has been completely charged, the voltage of C_{r2} is the same as that of C_2. Therefore, this condition provides the body diode of S_4 ZVS turn-on. At the end of mode 3, the voltage of C_{r2} reaches V_H. S_4 is turned on with ZVS and the current in L_{b1} continues. Thus, the energy transfers from the coupled inductor to the load by the body diode of S_4 in the next mode. The current stress of S_2 is obviously reduced. $i_{La1}= I_{La1(t2)}$, $i_{Lb1}=I_{Lb1(t2)}$ and $u_{Lb1}=U_{Lb1(t2)}$ are the initial conditions. For this resonance, the following equations are:

$$\begin{cases} C_{r2}\dfrac{dv_{Cr2}}{dt} = i_{Cr2} = i_{Lb1} \\ M\dfrac{di_{Lb1}}{dt} - L_{a1}\dfrac{di_{La1}}{dt} = 0 \\ M\dfrac{di_{La1}}{dt} = L_{b1}\dfrac{di_{Lb1}}{dt} + v_{Cr2} \end{cases} \tag{2}$$

Therefore: $$i_{DS1} = I_i - i_{La1} \tag{3}$$

$$i_{Lb1} = I_{Lb1(t2)} \cos \omega_{1(t2)} (t - t_2) + \sqrt{\frac{C_{r2}(L_{a1}L_{b1} - M^2)}{L_{a1}L_{b1}^2}} U_{Lb1(t2)} \sin \omega_{1(t2)} (t - t_2) \quad (4)$$

$$v_{Cr2} = I_{Lb1(t2)} \sqrt{\frac{C_{r2}(L_{a1}L_{b1} - M^2)}{L_{a1}}} \sin \omega_{1(t2)} (t - t_2) - \frac{C_{r2}(L_{a1}L_{b1} - M^2)}{L_{a1}L_{b1}} U_{Lb1(t2)} \cos \omega_{1(t2)} (t - t_2) \quad (5)$$

where $\omega_{1(t2)} = \sqrt{\frac{L_{a1}}{C_{r2}(L_{a1}L_{b1} - M^2)}}$

4) Mode 4 ($t_3 \le t < t_4$):

In this mode, S_1 is turned on. Because the current in L_{b1} falls to zero slowly, the body diode of S_4 is turned off with ZCS. Meanwhile, the freewheeling current i_{La1}–I_i in S_1 continues to decrease. At t=t_3, the initial conditions are v_{Cr2}=V_H, i_{La1}=$I_{La1(t3)}$ and i_{Lb1}=$I_{Lb1(t3)}$. The following equations are valid:

$$\begin{cases} -M \dfrac{di_{Lb1}}{dt} + L_{a1} \dfrac{di_{La1}}{dt} = 0 \\ L_{b1} \dfrac{di_{Lb1}}{dt} - M \dfrac{di_{La1}}{dt} = V_H \end{cases} \quad (6)$$

$$i_{La1} = I_{La1(t3)} - \frac{M}{L_{a1}L_{b1} - M^2} V_H (t - t_3) \quad (7)$$

$$i_{Lb1} = I_{Lb1(t3)} - \frac{M}{L_{a1}L_{b1} - M^2} V_H (t - t_3) \quad (8)$$

The interval before which i_{La1}–I_i fall to zero provides the ZVZCT turn-on margin for S_1. The signal of S_1 is applied in this margin when the body diode is active.

5) Mode 5 ($t_4 \le t < t_5$):

At the beginning of mode 5, S_2 is turned off. The turn-off current for S_2 is lower than I_i due to the resonance in mode 4. Furthermore, the voltage of S_2 is not directly raised to V_H. The ZVS-off of S_2 is realized due to C_{r2}. The current in L_{b1} and C_{r2} resonates. At t=t_4, the initial conditions are i_{Lb1}=$I_{Lb1(t4)}$, i_{La1}=$I_{La1(t4)}$, $v_{cr2(t4)}$=V_H, and v=$U_{Lb1(t4)}$. The following equations exist:

$$\begin{cases} M \dfrac{di_{Lb1}}{dt} - L_{a1} \dfrac{di_{La1}}{dt} - v_{cr2} + V_H = 0 \\ L_{b1} \dfrac{di_{Lb1}}{dt} - M \dfrac{di_{La1}}{dt} = v_{Cr2} \\ C_{r2} \dfrac{dv_{Cr2}}{dt} = i_{La1} - i_{Lb1} \end{cases} \quad (9)$$

Further derivation can be obtained as:

$$i_{Lb1} = \frac{(I_{La1(t4)} - I_{Lb1(t4)})(L_{a1} - M)^2 (L_{a1} + M)}{C_{r2}(L_{a1} + L_{b1} + 2M)(L_{a1}L_{b1} - M^2)} \cos \omega_{1(t4)} (t - t_4) - \sqrt{\frac{(L_{a1} + M)(M - L_{a1})}{(L_{a1} + L_{b1} + 2M)^2}} \left[(L_{a1} + L_{b1} + 2M) U_{Lb1(t4)} - V_H \right] \sin \omega_{1(t4)} (t - t_4) + \frac{V_H}{L_{a1} + L_{b1} + 2M} (t - t_4) + I_{Lb1(t4)} + \frac{(L_{a1} + M)(L_{a1} - M)^2}{L_{a1} + L_{b1} + 2M} (I_{Lb1(t4)} - I_{La1(t4)}) \quad (10)$$

where: $\omega_{1(t4)} = \sqrt{\frac{2M + L_{a1} + L_{b1}}{C_{r2}(L_{a1}L_{b1} - M^2)}}$.

6) Mode 6 ($t_5 \le t < t_6$):

This is a conventional PWM mode. In this mode, C_{r2} is discharged. Therefore, the voltage cross D_2, which is parallel to C_{r2}, also falls to zero, and D_2 conducts the current with ZVS. The inductor L_{b1} current falls to 0.

7) Mode 7 ($t_6 \le t < t_7$):

In this mode, the main switch is off and the capacitors C_{S1} and C_{S3} are separately charged and discharged. At t=t_6, v_{CS1}=0 and v_{Cs3}=V_H.

$$\begin{cases} v_{cs1} + v_{cs3} = V_H \\ i_{cs1} + i_{cs3} = I_i \\ i_{cs1} = C_{s1} \dfrac{dv_{cs1}}{dt} \\ i_{cs3} = C_{s3} \dfrac{dv_{cs3}}{dt} \end{cases} \quad (11)$$

In addition, the solution can be obtained by the equation group:

$$v_{Cs1} = \frac{I_i}{C_{s1} - C_{s3}} (t - t_6) \quad (12)$$

$$v_{Cs3} = V_H - \frac{I_i}{C_{s1} - C_{s3}} (t - t_6) \quad (13)$$

B. Buck Working Mode

For the buck mode, each operation stage of this topology is presented in Fig. 3(a). Fig. 3(b) shows the key waveforms of the buck mode. The seven operation stages for one PWM period have been analyzed below.

1) Mode 1 ($t_0 < t < t_1$):

Mode 1 is the PWM standard mode. At t = t_0, the main switch S_3 is off. L_1 and C_1 supply the output through the body-diode of S_1.

2) Mode 2 ($t_1 < t < t_2$):

At the beginning of mode 2, S_4 is activated. Resonance starts between C_{r2}, L_{a1}, L_{b1}, C_{S3} and C_{S1}. D_{S1} is turned off with ZVS because of the bypass capacitor C_{S1}. S_4 turns on with ZCS due to the coupling inductors. C_{S1} is charged to V_H, and C_{S3} is discharged. Thus, S_1 does not suffer from voltage stress. The initial conditions are v_{Cr2}=0, i_{La1}=i_{Lb1}=0, $v_{Cs1(t1)}$=0, $v_{Cs3(t1)}$=V_H and I_L=constant. The following equations are derived as:

$$\begin{cases} (L_{a1} - M)(C_{s3} - C_{s1}) \dfrac{d^2 i_{La1}}{dt^2} + (L_{b1} - M)(C_{s3} - C_{s1}) \dfrac{d^2 i_{Lb1}}{dt^2} = i_{La1} - I_{L1} \\ -C_{r2} M \dfrac{d^2 i_{La1}}{dt^2} + C_{r2} L_{b1} \dfrac{d^2 i_{Lb1}}{dt^2} + i_{Lb1} = I_{L1} \end{cases} \quad (14)$$

3) Mode 3 ($t_2 < t < t_3$):

In mode 3, resonance separately charges and discharges

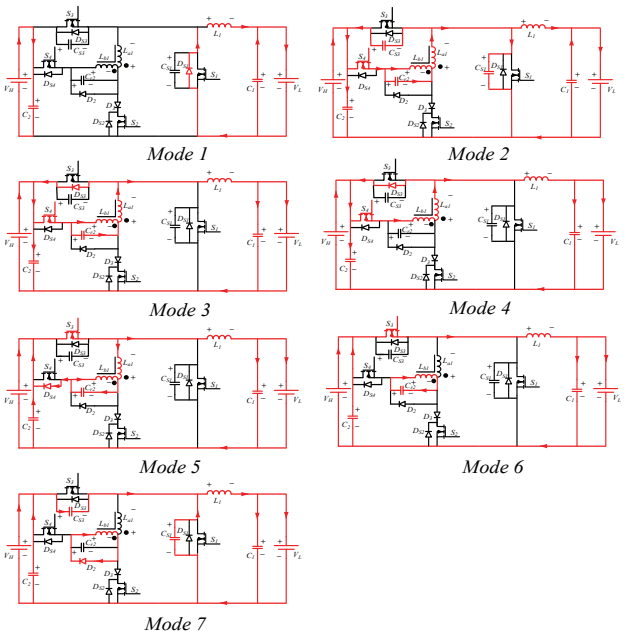

(a)

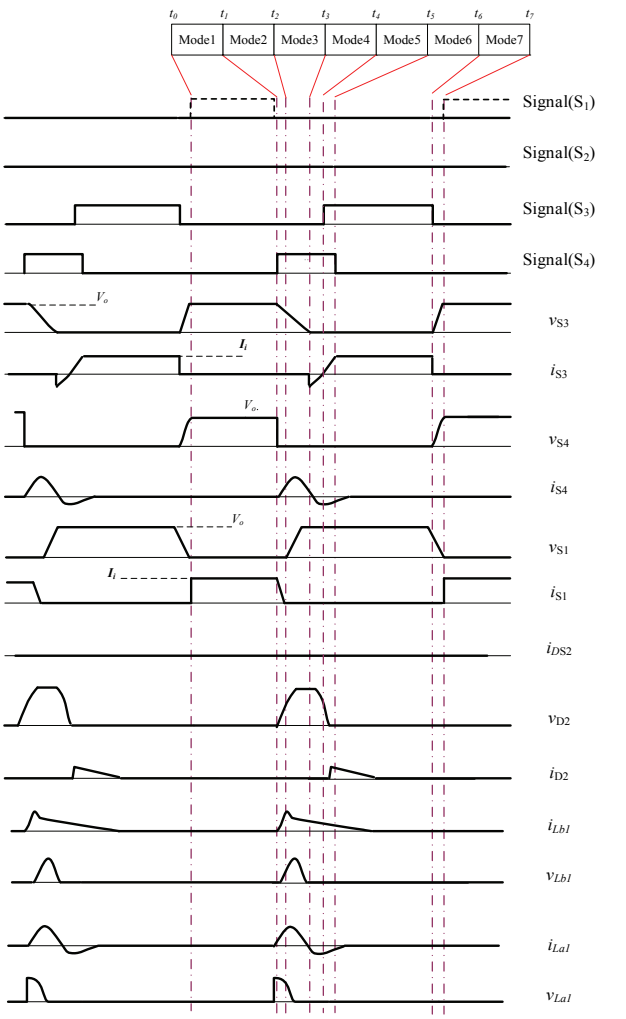

(b)

Fig. 3. Operations and principles for the buck mode: (a) Operation stages for the buck mode; (b) Key waveforms for the buck mode.

C_{S1} and C_{S3}. Later, D_{S3} is active with ZVS due to the bypass capacitor C_{S3}. L_{b1}, L_{a1} and C_{r2} continue to resonate through the anti-parallel-diode of S_3. The following initial values are valid: $v_{Cr2}= U_{Cr2(t2)}$, $i_{La1}= I_{La1(t2)}$, $i_{Lb1}= I_{Lb1(t2)}$ and $u_{Lb1}= U_{Lb1(t2)}$. The following formulas can be obtained:

$$\begin{cases} -M\dfrac{di_{La1}}{dt}+L_{b1}\dfrac{di_{Lb1}}{dt}+L_{a1}\dfrac{di_{La1}}{dt}-M\dfrac{di_{Lb1}}{dt}=0 \\ -M\dfrac{di_{La1}}{dt}+L_{b1}\dfrac{di_{Lb1}}{dt}=v_{cr2} \\ i_{Cr2}=C_{r2}\dfrac{dv_{Cr2}}{dt} \\ i_{Lb1}+i_{Cr2}=i_{La1} \end{cases} \tag{15}$$

The following conclusions are valid:

$$\begin{aligned} i_{Lb1} &= \frac{\sqrt{C_{r2}(L_{a1}L_{b1}-M^2)}}{\sqrt{L_{a1}+L_{b1}-2M}\,L_{b1}}U_{Lb1(t2)}\sin\omega_{2(t2)}(t-t_2) \\ &-\frac{(L_{a1}-M)(I_{La1(t2)}-I_{Lb1(t2)})}{L_{a1}+L_{b1}-2M}\cos\omega_{2(t2)}(t-t_2) \\ &+\frac{L_{a1}-M}{L_{a1}+L_{b1}-2M}I_{La1(t2)}+\frac{L_{b1}-M}{L_{a1}+L_{b1}-2M}I_{Lb1(t2)} \end{aligned} \tag{16}$$

where: $\omega_{2(t2)}=\sqrt{\dfrac{L_{a1}+L_{b1}-2M}{C_{r2}(L_{a1}L_{b1}-M^2)}}$.

4) Mode 4 ($t_3 < t < t_4$):

For this mode, C_{r2} has been completely charged. The current in L_{a1} and L_{b1} continues to flow through D_{S3}. t_4-t_2 are the ZVT interval for S_3. At the end of mode 4, the current in L_{a1} and L_{b1} decreased to 0. The initial conditions are: $v_{Cr2}= v_{Cr2(t3)}$ and $i_{La1}= i_{Lb1}= I_{La1(t3)}$.

$$-M\frac{di_{La1}}{dt}+L_{b1}\frac{di_{Lb1}}{dt}+L_{a1}\frac{di_{La1}}{dt}-M\frac{di_{Lb1}}{dt}=0 \tag{17}$$

From the differential equation, it can be seen that in this mode, i_{Lb1} is close to the constant current $I_{La1(t3)}$. Then the interval of this mode should not be too long. Otherwise, there are serious circulation losses. This means that once the diode of the auxiliary switch and the main switch are active, the main switch should be turned on as soon as possible.

5) Mode 5 ($t_4 < t < t_5$):

When this mode starts, the main switch S_3 is turned on. C_{r2} starts to discharge, and C_{r2} resonates with L_{a1} and L_{b1}. This resonance provides S_4 with ZCS. The active signal is removed when this mode ends. The initial conditions are as follows : $v_{Cr2}= V_H$ and $i_{La1}= i_{Lb1}= 0$.

$$\begin{cases} v_{Cr2}-M\dfrac{di_{La1}}{dt}+L_{b1}\dfrac{di_{Lb1}}{dt}=0 \\ i_{Cr2}=C_{r2}\dfrac{dv_{Cr2}}{dt} \\ i_{Cr2}=i_{La1}+i_{Lb1} \end{cases} \tag{18}$$

Then:

$$i_{Lb1}=\frac{\sqrt{C_{r2}(L_{a1}L_{b1}-M^2)}}{\sqrt{L_{a1}+L_{b1}+2M}\,L_{b1}}U_{Lb1(t4)}\sin\omega_{2(t4)}(t-t_4)+\frac{(L_{a1}+M)(I_{La1(t4)}+I_{Lb1(t4)})}{L_{a1}+L_{b1}+2M}\cos\omega_{2(t4)}(t-t_4)+\frac{(L_{b1}+M)I_{Lb1(t4)}-(L_{a1}+M)I_{La1(t4)}}{L_{a1}+L_{b1}+2M} \quad (19)$$

where: $\omega_{2(t4)}=\sqrt{\frac{L_{a1}+L_{b1}+2M}{C_{r2}(L_{a1}L_{b1}-M^2)}}$

6) Mode 6 ($t_5 < t < t_6$):

Mode 6 is the PWM standard mode, where V_H supplies the output through L_1. Meanwhile, C_{r2} and L_{b1} are oscillating. The initial conditions are as follows: $v_{Cr2}= U_{Cr2(t5)}$ and $i_{Lb1}= I_{Lb1(t5)}$. The following equations can be obtained:

$$\begin{cases}-v_{Cr2}+L_{b1}\dfrac{di_{Lb1}}{dt}=0\\ i_{Cr2}=C_{r2}\dfrac{dv_{Cr2}}{dt}\\ i_{Cr2}=-i_{Lb1}\end{cases} \quad (20)$$

Then:

$$i_{Lb1}=\sqrt{\frac{C_{r2}}{L_{b1}}}U_{Lb1(t5)}\sin\omega_{2(t5)}(t-t_5)+I_{Lb1(t5)}\cos\omega_{2(t5)}(t-t_5) \quad (21)$$

$$u_{Lb1}=\sqrt{L_{b1}C_{r2}}\,\omega_{2(t5)}U_{Lb1(t5)}\cos\omega_{2(t5)}(t-t_5)-I_{Lb1(t5)}\omega_{2(t5)}L_{b1}\sin\omega_{2(t5)}(t-t_5) \quad (22)$$

where: $\omega_{2(t5)}=\frac{1}{\sqrt{C_{r2}L_{b1}}}$

7) Mode 7 ($t_6 < t < t_7$):

In this mode, L_{b1} releases the rest of the energy. At the same time C_{S1} and C_{S3} are charged and discharged by the constant current I_{L1}. When this is completed, one circle is over and the next period starts. The initial conditions for this mode are: v_{CS3}=0 and v_{CS1}=V_H.

$$\begin{cases}v_{Cs1}+v_{Cs3}=V_H\\ i_{Cs3}+i_{Cs1}=I_{L1}\\ i_{Cs3}=C_{s3}\dfrac{dv_{Cs3}}{dt}\\ i_{Cs1}=C_{s1}\dfrac{dv_{Cs1}}{dt}\end{cases} \quad (23)$$

Thus, the solution can be expressed as:

$$v_{Cs1}=\frac{I_{L1}}{C_{s1}-C_{s3}}(t-t_6) \quad (24)$$

$$v_{Cs3}=V_H-\frac{I_{L1}}{C_{s1}-C_{s3}}(t-t_6) \quad (25)$$

III. Parameter Analysis and Topology Design

A. ZVZCT Turn-On Conditions and ZVS Turn-Off Conditions for the Main Switch

The ZVS off condition of S_1 can always be met due to the bypass capacitor C_{S1}. On the other side, before the activate signal of S_2 is off, C_{S1} must be completely discharged in the boost working mode. At this time, the body diode of S_1 starts to conduct current, the driving signal of the main switch (S_1) is activated, and the main switch turns on at ZVZCT. In this case, the discharge interval of C_{S1} and C_{S3} should not exceed t_3-t_2. Therefore, the following constraints must be implemented for the ZVZCT turn-on of S_1, with consideration of the charge and discharge current of C_{S1} and C_{S3}:

$$i_{La1(t3)}-I_i\geq 0 \quad (26)$$

where I_i is the input current, and $i_{La1(t3)}$ is the current in L_{a1} for mode 3.

i_{La1} creates the ZVS condition for the main switch. When at a light load, the circulating current is larger, while at a heavy load, the circulating current is smaller. The reason for reserving a current margin in the design is to prevent a soft switch lost in the case of i_{La1}-I_i<0 due to a system overload. This resonant current and the voltage on i_{S1} do not form an overlap. Thus, there is no power loss for this part.

With the consideration above, the load range can be estimated. If the load changes beyond the designed range, soft switching is lost, the main switch goes into the HS mode, and there is a voltage shock at the main switch. Some circuits that do not work properly in the HS conditions can be damaged.

$$C_{S1}+C_{S3}\leq\frac{I_i}{V_o}(t_3-t_2) \quad (27)$$

The turn-on signal of the main switch should delay the auxiliary switch. The delay time should be limited by the conditions below:

$$\begin{cases}(t_3-t_1)<t_{delay}<t\big|_{iDs1=0} & \text{in boost mode}\\ (t_3-t_1)<t_{delay}<t\big|_{iDs3=0} & \text{in buck mode}\end{cases} \quad (28)$$

where $t\big|_{iDs1=0}$, $t\big|_{iDs3=0}$ is the moment when i_{DS1}, i_{DS3} decreases to 0, and t_3 is the moment when the voltage of C_{S1} and C_{S3} resonate to 0.

In the buck mode, to achieve ZVZCT turn-off for S_4, the resonance should satisfy the following constraint:

$$\frac{1}{2}C_{r2}V^2_{Cr2(t4)}\geq\frac{1}{2}L_{a1}i^2_{La1(t4)} \quad \text{in buck mode} \quad (29)$$

The delay relation between the auxiliary switch and the main switch is related to the load and voltage changes. The main part of the reverse recovery current, i_a-I_i, is the key factor in creating the main switch ZVZCT.

I_i is another important factor that determines the delay time. With the consideration of (16) and (27), the following relation

can be obtained:

$$t_{delay} > (t_3 - t_1) > (t_3 - t_2) > \frac{(C_{S1} + C_{S3})V_o}{I_i} \quad (30)$$

If the main switch voltage is unable to fall back to zero due to factors such as signal mismatch, current chock occurs on the main switch.

The duty cycle D of the conventional buck-boost circuit can affect the soft switching. A D satisfying the following conditions can achieve soft switching:

$$\begin{cases} D = \dfrac{V_o - V_i}{V_o} \\ V_o I_o = V_i I_i \\ i_{S1\_\max} - I_i \geq 0 \\ Gain = \dfrac{V_o}{V_i} \end{cases}, \text{ then } Gain \leq \frac{i_{S1\_\max}}{I_o} \quad (31)$$

$$\text{Obviously, } Gain \geq \frac{T - t_{delay}}{T}$$

The buck mode has a similar conclusion.

If the coupling inductance is not reset, the diode D_2 works in the hard switching mode. This forces the inductor to reset when there is still a current flow, which is not desirable. Thus, appropriate circuit parameters are needed to avoid this situation.

The time margin of the reset is $t_m \approx T - t_{on\_aux} - t_{release} > 0$. Most of the energy in the capacitor C_{r2} is transferred to L_{b2} and is eventually released through D_2. By the equations below, t_m can be calculated by:

$$t_{release} = \frac{\frac{1}{2}C_{r2}V_{Cr2(t4)}^2}{(\frac{1}{2}I_{Lb1(MAX)})^2 R} = \frac{I_{Lb1(MAX)} - 0}{L_{b1}} \quad (32)$$

$$\text{Therefore, } t_m \approx T - t_{on\_aux} - \sqrt[3]{\frac{2C_{r2}V_{Cr2(t4)}^2}{RL_{b1}^2}} > 0 \quad (33)$$

where, $v_{Cr2\ (t4)}$ is the voltage after C_{r2} is charged, R is the internal resistance of the loop in mode 6, and t_{on_aux} is the pulse width of the auxiliary switch.

B. Coupled Inductor for Soft-Switching Realization

For the proposed topology, the main loop is quite independent. It can adapt to a wide load range. The coupling inductors enable the main switch to acquire soft switching, and assist the auxiliary switch to achieve ZVS or ZCS. The stress on the auxiliary switch can be well controlled by adjusting the coupling coefficient. Therefore, the design of the coupling inductors for this circuit is needed.

Coupled inductors use high frequency iron core materials, such as MnFe204, ZnFe204, etc. In practice, the coupling coefficient of a ring-type core is difficult to reach 0.95. The coupling coefficient varies with the distance between the two windings. Adjustable coupling coefficients can be obtained by adjusting the distance between the two windings.

The coupling coefficient and the values of L_{a1} and L_{b1} have a major impact on the circuit. Therefore, in the initial design stage, the magnetic core is an important part. The related parameters are designed as follows.

The initial conditions are: window fill factor: K_o=0.4; core fill factor (ferrite): K_c=1; working flux density of the transformer: $B_m \leq 1/2\ B_{sat}$; current density (the value for natural cooling): j=4.2 A/mm^2; switching frequency: f_{sw}=100 kHz; output voltage: V_{out}=200 V; input voltage: V_{in}=120 V; and auxiliary switch turn-on interval: T_{on_max}=1 *us*.

In this design, the OR48X30X15 type is selected. Then A_e = 133 mm^2, A_w=1.75 mm^2, L_e=118 mm and V_e=15700 mm^3. In addition, the saturation magnetic density of the ferrite core B_{sat} = 3900 G. Thus, B_m = 1900 G.

According to simulations: P_o=0.000375 W and I_{La1_max}=12 A. Then:

$$L_{a1} \approx \frac{V_{\text{in}} \times T_{on}}{I_{La1\_\max} \times f_{sw}} = \frac{120 \times 0.1}{12 \times 10^5} = 10uH \quad (34)$$

$$N_p = \frac{V_{\min} \times t_{on\max}}{A_e \times B_m} = \frac{120 \times 10}{133 \times 2} = 4.5 \quad (35)$$

Due to topology design requirements: $L_{a1} \leq 8\ uH$, it is necessary to take 4 turns. Since the coupling inductance does not want to introduce a higher output voltage (stress), the parameters could be determined according to the features of the circuit topology: $L_{b1} \approx L_{a1}$. Thus, L_{b1}=6 *uH*.

$$AP_p = \frac{P_o \times 10^6}{2\eta \times K_o \times K_c \times f_s \times B_m \times j} = \frac{370 \times 10^{-6} \times 10^6}{2 \times 0.8 \times 0.4 \times 1 \times 100000 \times 1900 \times 4.2} cm^4 \quad (36)$$

$$AP = A_w \times A_e = 1.33cm^2 \times 0.0175cm^2 \quad (37)$$

$AP > AP_p$. The design meets the requirements.

The coupling coefficient has a great influence as: 1) the magnitude of the resonant circulation, 2) the realization of the ZVS boundary. It is observed from Fig. 4(a), that once the coupling coefficient exceeds 0.9, S_2 and S_4 suffer from unacceptable peak currents in both the boost and buck modes. If the coupling coefficient is less than 0.5, the ZVZCT in S_4 is lost in the buck mode. Therefore, the best choice is: the maximum current in S_2. In addition, S_4 and ZVZCT of S_4 should both be considered in the buck mode.

Consequently, the following equations become available:

$$\begin{cases} i_{La1} - I_i = I_{La1(t3)} - \dfrac{M}{L_{a1}L_{b1} - M^2} V_H (t - t_3) - I_i \geq 0 \\ k \in [0.5\ ,\ 0.9] \\ k = \dfrac{M}{\sqrt{L_{a1}L_{b1}}} \end{cases} \quad (38)$$

Most of the parameters need to be adjusted in the process of experiments. However, some of the parameters can be

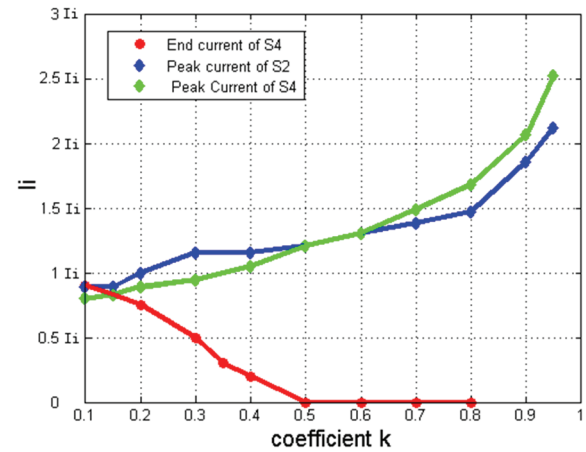

(a)

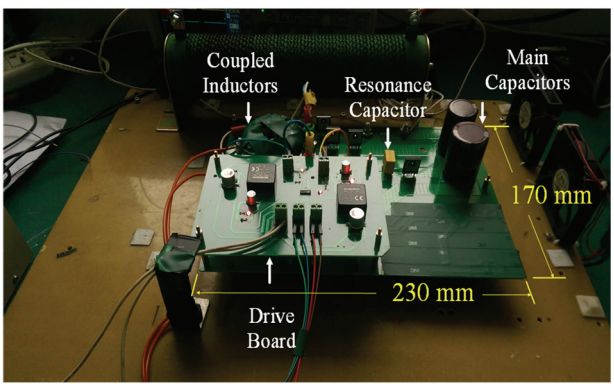

(b)

Fig. 4. Coupling effect for the circuit and the proposed DC/DC converter: (a) Coefficient effect on S_2 and S_4; (b) Proposed converter.

estimated by the analysis. Considering that the resonance among C_{S1}, C_{S3}, the coupled inductor and C_{r1} occurs in mode 2 of the boost case, C_{r2} needs to choose a value with the same level (1-10nF). With equation (15), L_{a1} can be estimated with the assumption of $V_{Cr2(t4)}$=V_H (200 V), $i_{La1(t4)}$=I_i (the reverse current cannot be too large) and C_{r1}=5 nF, the relation can be calculated as L_{a1}≤8 uH. Therefore, L_{b1} should choose the same level (1-10 uH). On the other hand, the coupled inductor has the dotted terminals connected together, and the coefficient k choses the value of 0.8 with consideration of Fig. 4.

With the equation 15, (t_3-t_2) should be larger than 272 ns with the assumption of V_o=200 V and I_i=5 A. Therefore, with consideration of t_{delay} > (t_3-t_1) > (t_3-t_2), the parasitic capacitance and the switch characteristics, t_{delay}=1 us. In this coupling inductor design, the value of the coupling inductance is determined first. Then the turn ratio is determined. Therefore, it can meet the soft switching requirement in terms of bidirectional resonance. In addition, the turn ratio of the coupling inductor can also be decided.

C. Switching Loss Distribution

Based on the circuit parameters determined above, it is possible to theoretically estimate the main power distribution of the converter as shown in Fig. 5 below.

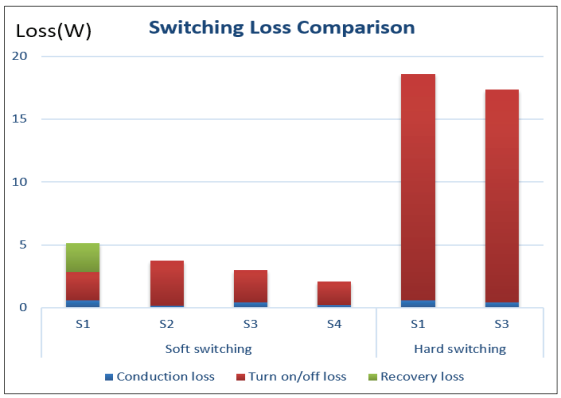

(a)

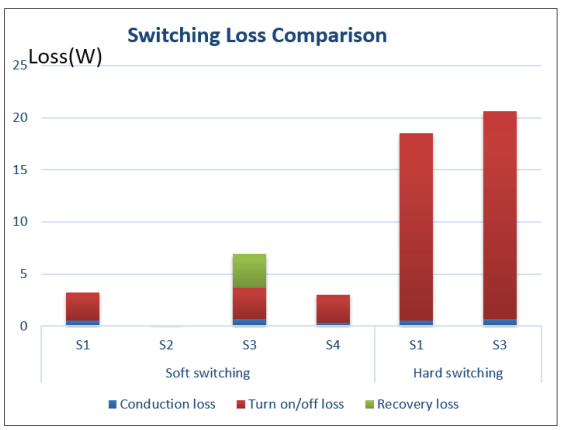

(b)

Fig. 5. Switching loss comparison: (a) Boost mode at full load; (b) Buck mode at full load.

TABLE I
EXPERIMENTAL CONDITIONS AND CIRCUIT PARAMETERS

Symbols	Descriptions	Specifications
S_1, S_3	Main switch	IPW60R041C6
S_2, S_4	Auxiliary switch	IXFK55N50
D_2, D_3	Diodes	RHRP30120
C_{r2}	Resonant capacitors	5 nF
L_{a1}, L_{b1}	Coupled inductors	8 μH, 6 μH
k_{ab}	Coupling coefficients	0.8

Thus, the converter loss comes mainly from the switching devices, and the switch loss comes mainly from the turn-on/turn-off moment. Theoretically, it can be seen that the power cost advantage of soft switching is obvious.

IV. EXPERIMENTAL RESULTS

In order to verify the above analysis, a prototype of the proposed converter has been established. Table I lists the components and circuit parameters of the converter.

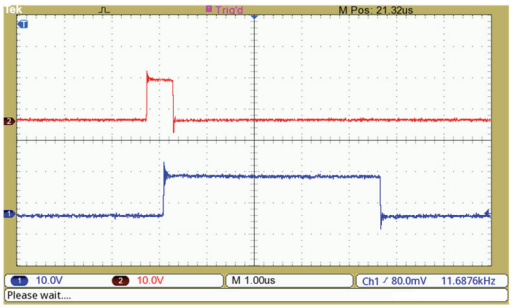

(a)

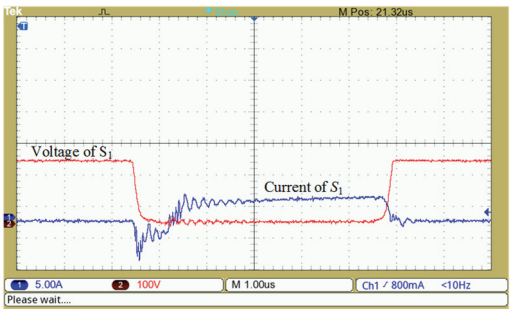

(b)

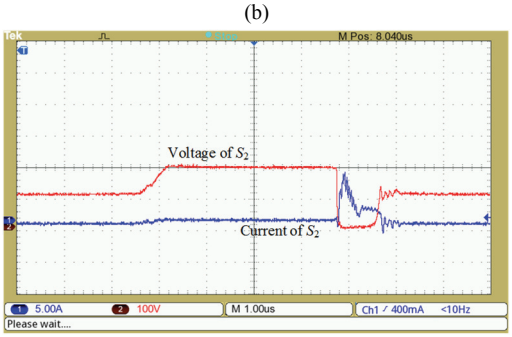

(c)

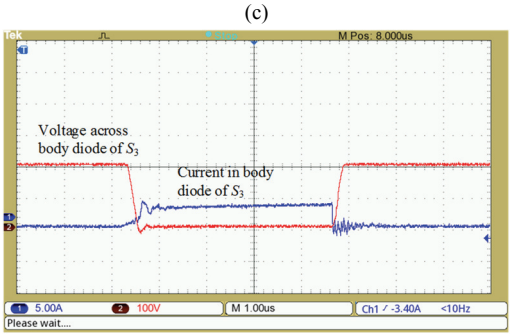

(d)

Fig. 6. Voltage and current for S_1, S_2 and S_3 in the boost mode (switching frequency100 kHz, 120/200 V, 500 W): (a) Drive signals of the main and auxiliary switches; (b) Voltage and current of S_1; (c) voltage and current of S_2; (d) Voltage and current of S_3.

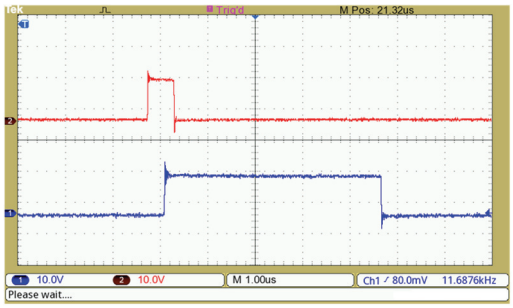

(a)

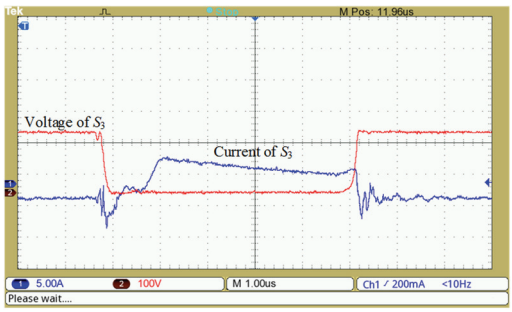

(b)

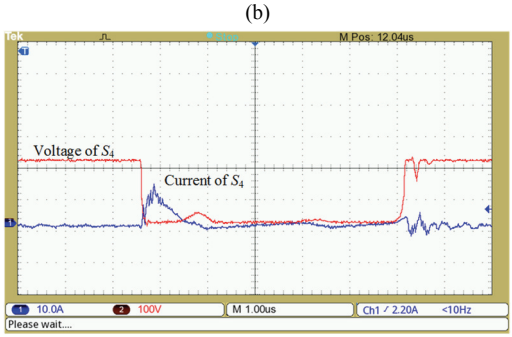

(c)

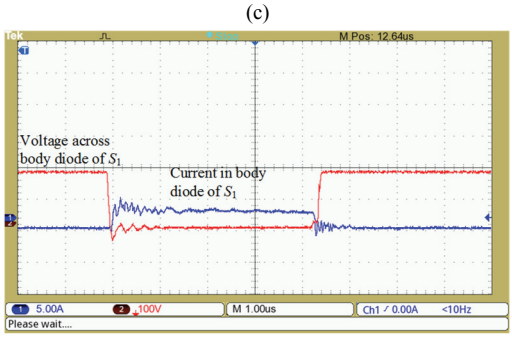

(d)

Fig. 7. Voltage and current for S_3, S_4 and S_1 in the buck mode (switching frequency100 kHz, 120/200 V, 500 W): (a) Drive signals of main and auxiliary switches; (b) Voltage and current of S_3; (c) voltage and current of S_4; (d) Voltage and current of S_1.

A photo of the proposed converter prototype is shown in Fig. 4(b). This converter is composed of a main inductor (L_1), the coupled inductors, the capacitor C_{r2}, and four transistors with body diodes. The output capacitance is 560 uF. The switching frequency of the converter is 100 kHz. The low and high voltages are 120 V and 200 V, respectively. The test power is 500 W.

In the boost mode, control signals are presented in Fig. 6(a), and the processes of the turn-on and turn-off of the main switch are shown in Fig. 6(b). In this figure, v_{S1} is reduced to zero, and the enable signal is applied to S_1. Then the current reverses, and increases from zero. Thus, the S_1 ZVZCT turn-on is realized. Once the disable signal is applied, i_{S1} is rapidly reduced to zero, and v_{S1} increases. Therefore, S_1 also realizes ZVS during the turn-off process.

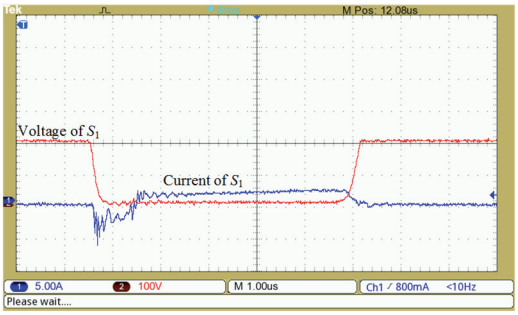

(a)

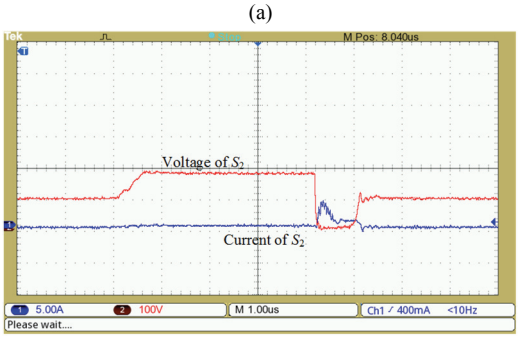

(b)

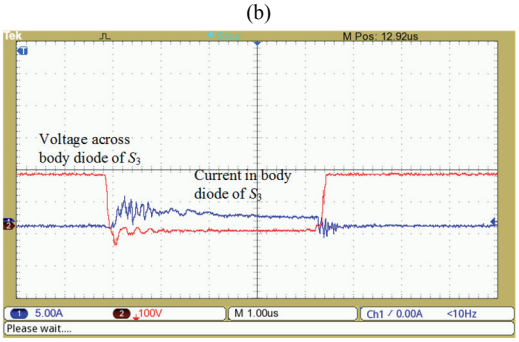

(c)

Fig. 8. Voltage and current for S_1, S_2 and S_3 in the boost mode (switching frequency100 kHz, 120/200 *V*, 150 *W*): (a) Voltage and current of S_1; (b) Voltage and current of S_2; (c) Voltage and current of S_3.

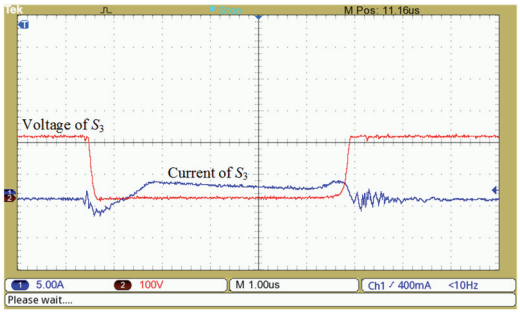

(a)

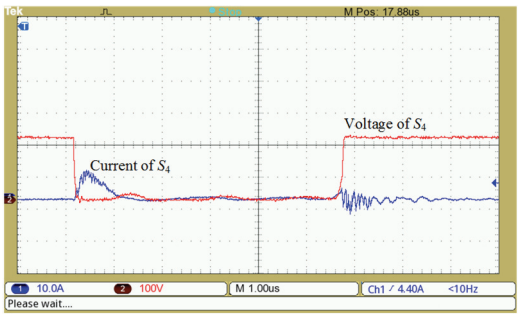

(b)

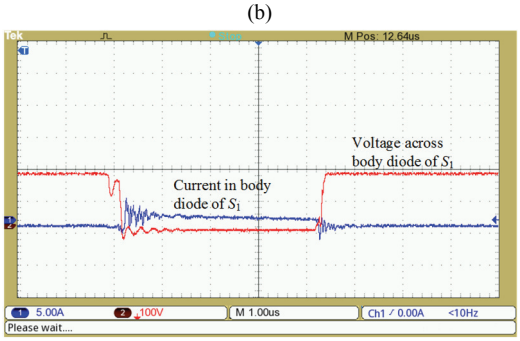

(c)

Fig. 9. Voltage and current for S_3, S_4 and S_1 in the buck mode (switching frequency100 kHz, 120/200 *V*, 150 *W*): (a) Voltage and current of S_3; (b) Voltage and current of S_4; (c) Voltage and current of S_1.

The switching process of S_2 is shown in Fig. 6(c). The S_2 current increases slowly when the active signal of S_2 is applied. The coupling inductors are helpful for transferring power to the output side of the converter. Due to the coupling effect, S_2 decreases rapidly. Therefore, the smaller average current of S_2 reduces the circulating loss when compared with the common inductor. It can also be observed in Fig. 6(c), that when the switching signal of S_2 is removed, the ZVS and the lower i_{S2} and v_{S2} make S_2 have a good turning off.

As shown in Fig. 6(d), the main diode (body diode of S_3) in the boost mode operates for soft switching. Therefore, the boost efficiency is improved.

As can be seen in Fig. 7(b), v_{S3} reduces to "0" before the activation signal of S_3 is applied. Then the current of S_3 reverses and increases from "0". Therefore, S_3 is able to turn on with ZVZCT. When the signal for S_3 is turned off, the zero voltage switch is realized during the turn-off process. In Fig. 7(b), there exists a small overlap in the turn-off, because C_{S3} only includes the S_3 parasitic capacitor. Therefore, the voltage raises quickly. However, this does not get the voltage shock, and it does not significantly increase the power loss. If C_{S3} increases, this overlap can be avoided. Therefore, choosing a switch component with a larger C_{S3} may be a solution, while getting an additional parallel capacitor is not recommended.

The turn-on and turn-off processes for S_4 are shown in Fig. 7(c). The current of S_4 increases slowly when the active signal of S_4 is on. Therefore, S_4 turns on with ZCS. Due to the coupling effect, before the signal is removed, the current of S_4 resonates to zero and ZVZCT is realized.

In Fig. 7(d) a fly-back diode (body diode of S_1) in the buck mode operates under soft switching.

Fig. 8(a) shows that main switch turns on with ZVZCT and turns off with ZVS in the boost mode at a low power level.

In Fig. 8(b), the auxiliary switches turn on with ZCS and turn off with ZVS in the boost mode at a low power level.

As shown in Fig. 8(c), the body diode of S_3 is in the soft

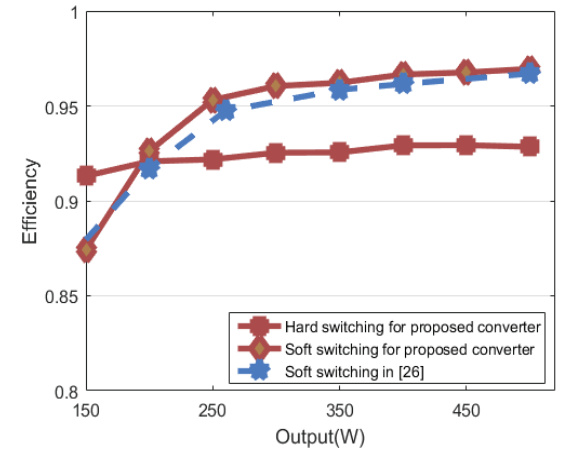

(a)

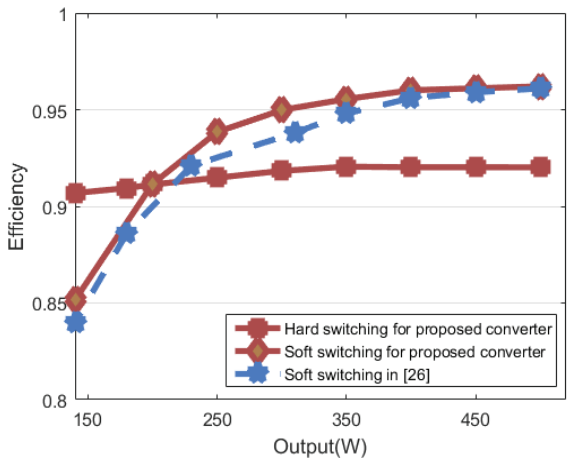

(b)

Fig. 10. Efficiency comparisons for: (a) Boost mode; (b) Buck mode.

switching state in the boost mode at a low power level.

It can be seen from Fig. 9(a), that S_3 turns on with ZVZCT and turns off with ZVS in the buck mode at a low power level.

The switch S_4 in Fig. 9(b) is turned on with ZCS and turned off with ZVZCT in the buck mode at a low power level.

It is shown in Fig. 8(c) that soft switching for the body diode of S_1 is obtained for a light load.

The efficiency of the proposed bi-directional converter is tested by a power analyzer (WT-1800) in the boost and buck modes. Efficiency comparison curves for the proposed converter, hard switching and another topology are shown in Fig. 10(a) and (b). These figures show that a high efficiency can be achieved at a full load.

At a full load, the peak efficiency reaches 97% and 96.4% in the boost and buck mode for the proposed converter. That is consistent with the fact that the energy in the resonance tank can be delivered to the output and reduce the auxiliary switch average conduction current, due to the coupling inductors.

TABLE II
TOPOLOGY FEATURES AND COMPARISON OF OTHER CONVERTERS

	[17]	[18]	[26]	Proposed
Affect to main circuit	Serious	Medium on current	Serious	Small
External devices	4	5	2	6
Load range	40%-100%	Not involved	Not involved	30%-100%
Stress	No stress	Medium current stress	Small current s tress	No voltage stress
Efficiency	Boost: 96.2% Buck: 94.3%	Boost: 91.5% Buck: 91%	Boost: 96.5% Buck: 96.03%	Boost: 97% Buck: 96.4%

In [26], the topology is designed for coupling with a main inductor. The resonance inductor is coupled with the main inductor which leads to a large reverse current. Furthermore, an unnecessary oscillation that is not from parasites or stray parameters occurs in the main circuit. This oscillation may cross zero at a low power level. These problems are caused by the resonance and main circuit coupling. For the above reasons, the efficiency at a low power level is not very good.

Another problem with [26], is that the design margin of the coupling inductance parameters is narrow. The soft-switching conditions is depended on a temporary equivalent electromotive force generated by the coupling effect to release the bypass capacitor of the switch. This electromotive force is a function of the main circuit current changing rate, which means that a large ripple must exist in the main circuit to ensure soft switching. Therefore, the ripple rate and soft switch is a pair of contradictions that cannot both occur.

Table II compares a number of topologies including [26]. From this comparison, it is easier to find the features and application scope of each topology.

V. CONCLUSION

For this study, a new bi-directional ZVZCT soft-switching converter is proposed. The converter provides the main switch with ZVZCT during the turn-on process and ZVS during the turn-off process, regardless the power flow direction. In addition, the auxiliary switches operate at soft switching due to the coupled inductor. The main diodes can work with soft switching. The main switch does not suffer from additional voltage and current stresses. Furthermore, for the auxiliary switch, the current stress is limited to an acceptable level. A prototype is built, and experimental results verify the realization of the soft switch. This is in accordance with the theoretical analysis derived in this paper.

ACKNOWLEDGMENT

This work was supported by National Science Fund of China (51677118), National Key R&D Plan Key Special Project (2017YFE0102000), Shanghai Municipal Inter-Governmental International Collaboration Project (16510711500) and the International Science & Technology Cooperation Program of China (2016YFE0102200).

REFERENCES

[1] P. Thounthong, "Control of a three-level boost converter based on a differentia flatness approach for fuel cell vehicle applications," *IEEE Trans. Veh. Technol.*, Vol. 61, No. 3, pp. 1467-1472, Mar. 2012.

[2] C.-E. Kim, S.-K. Han, K.-B. Park, and G.-W. Moon, "A new high efficiency ZVZCS bidirectional dc/dc converter for HEV 42V power systems," *J. Power Electron.*, Vol. 6, No. 3, pp. 271-278, Jul. 2006.

[3] N. Molavi, E. Adib, and H. Farzanehfard, "Soft-switching bidirectional DC-DC converter with high voltage conversion ratio," *IET Power Electron.*, Vol. 11, No. 1, pp. 33-42, 2018.

[4] V. V. S. K.Bhajana, P. Drabek, and P. K. Aylapogu, "A novel ZVS non-isolated bidirectional DC-DC converter for energy storage systems," *IECON*, pp. 663-668, 2017.

[5] H. Liu, L. Wang, F. Li, and Y. Ji, "Bidirectional active clamp DC-DC converter with high conversion ratio," *Electron. Lett.*, Vol. 53 No. 22 pp. 1483-1485, 2017.

[6] D. Y. Jung, Y. H. Ji, S. H. Park, Y. C. Jung, and C. Y. Won, "Interleaved soft-switching boost converter for photovoltaic power-generation system," *IEEE Trans. Power Electron.*, Vol. 26, No. 4, pp. 1137-1145, Apr. 2011.

[7] H. Choi, M. Jang, and V. G. Agelidis, "Zero-current-switching bidirectional interleaved switched-capacitor DC-DC converter: analysis, design and implementation," *IET Power Electron.*, Vol. 9, No. 5, pp. 1074-1082, 2016.

[8] K. Jin, M. Yang, X. Ruan, S. Member, and M. Xu, "Three-level bidirectional converter for fuel-cell/battery hybrid power system," *IEEE Trans. Ind. Electron.*, Vol. 57, No. 6, pp. 1976-1986, Jun. 2010.

[9] M. Aamir and H.-J. Kim, "Analysis of ZVS non-isolated bidirectional DC-DC converter," *Circuits and Systems (MWSCAS),* pp. 1-4, 2011.

[10] J. K. Eom, J. G. Kim, J. H. Kim, S. T. Oh, Y. C. Jung, and C. Y. Won, "Analysis of a novel soft switching bidirectional DC-DC converter," *J. Power Electron.*, Vol. 12, No. 6, pp. 859-868, Nov. 2012.

[11] R. N. D. Prado, "A new ZVT PWM converter family: analysis, simulation and experimental results," *APEC*, pp. 978-983, 1994.

[12] W. Han and L. Corradini, "Accurate ZVS boundary analysis for bidirectional dual-bridge series resonant DC-DC converters," *Control and Modeling for Power Electronics (COMPEL)*, 2017.

[13] A. F. Bakan, H. Bodur, and I. Aksoy, "A novel ZVT-ZCT PWM DC-DC converter," in *Proc. 11th Eur. Conf. Power Electron. (EPE)*, 2005.

[14] P. Das and G. Moschopoulos, "A comparative study of zero-current transition PWM converters," *IEEE Trans. Ind. Electron.*, Vol. 54, No. 3, pp. 1319-1328, Jun. 2007.

[15] B. Akın and H. Bodur," A new single-phase soft-switching power factor correction converter," *IEEE Trans. Power Electron.*, Vol. 26, No. 2, pp. 436-443, Feb. 2011.

[16] H. Mao, F. C. Y. Lee, X. Zhou, H. Dai, M. Cosan, and D. Boroyevich," Improved zero-current transition converters for high-power applications," *IEEE Trans. Ind. Appl.*, Vol. 33, No. 5, pp. 1220-1232, Sep./Oct. 1997.

[17] P. Das, B. Laan, and S. A. Mousavi, "A nonisolated bidirectional ZVS-PWM active clamped DC-DC converter," *IEEE Trans. Power Electron.*, Vol. 24, No. 2, pp. 553-558, Feb. 2009.

[18] P. Das, S. A. Mousavi, and G. Moschopoulos, "Analysis and design of a nonisolated bidirectional ZVS-PWM DC-DC converter with coupled inductors," *IEEE Trans. Power Electron.*, Vol. 25, No. 10, pp. 2630-2641, Oct. 2010.

[19] M. Aamir, S. Mekhilef, and H. J. Kim, "High-gain zero-voltage switching bidirectional converter with a reduced number of switches," *IEEE Trans. Circuits Syst. II*: *Exp. Briefs*, Vol. 62, No. 8, pp. 816-820, Aug. 2015.

[20] Y. T. Chen, S. M. Shiu, and R. H. Liang, "A new family of zero-voltage-transition nonisolated bidirectional converters with simple auxiliary circuit," *IEEE Trans. Ind. Electron.*, Vol. 63, No. 3, pp.1519-1527, Mar. 2016.

[21] I. Aksoy, H. Bodur, and A. F. Bakan, "A new ZVT-ZCT-PWM DC-DC converter," *IEEE Trans. Power Electron.*, pp.2093-2105, Aug. 2010.

[22] W. Yu, H. Qian, and J. S. Lai., "Design of high-efficiency bidirectional DC-DC converter and high-precision efficiency measurement," *IEEE Trans. Power Electron.*, Vol. 25, No. 3, pp. 650-658, Mar. 2010.

[23] G. Chen, Y. Deng, L. Chen, Y. Hu, L. Jiang, X. He, and Y. Wang, "A family of zero-voltage-switching magnetic coupling nonisolated bidirectional DC-DC converters," *IEEE Trans. Ind. Electron.*, Vol. 64, No. 8, pp. 6223-6233, Aug. 2017.

[24] H. Wu, J. Lu, W. Shi, and Yan Xing, "Nonisolated bidirectional DC-DC converters with negative-coupled inductor," *IEEE Trans. Power Electron.*, Vol. 27, No. 5, pp. 2231-2235, May 2012.

[25] R. L. Lin, Y. Zhao, and F. C. Lee, "Improved soft-switching ZVT converters with active snubber," *13th APEC*, pp. 1063-1069, 1998.

[26] L. Jiang, C. C. Mi, S. Li, M. Zhang, and X. Zhang, "A novel soft-switching bidirectional DC-DC converter with coupled inductors," *IEEE Trans. Ind. Appl.*, Vol. 49, No. 6, pp. 2730-2740, Jun. 2013.

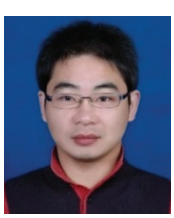

Wei Qian received his B.S. degree in Mechanical Engineering and Automation, and his M.S. degree in Aircraft Design from the Nanjing University of Aeronautics and Astronautics (NUAA), Nanjing, China, in 2005 and 2013, respectively. He is presently a Ph.D. candidate in the School of Mechanical Engineering, Shanghai Jiao Tong University (SJTU), Shanghai, China. His current research interests include soft switching power converters, power electronics devices and electric motor control systems for alternative-fuel vehicles.

Xi Zhang received his B.S. degrees in Applied Mathematics and in Information and Control Engineering, and his M.S. and Ph.D. degrees in Power Electronics and Electric Power Drives from Shanghai Jiao Tong University (SJTU), Shanghai, China, in 2002, 2004 and 2007, respectively. From September 2007 to July 2009, he held a postdoctoral position in the Department of Electrical and Computer Engineering, University of Michigan-Dearborn, Dearborn, MI, USA. He is presently working as a Professor in the Institute of Automotive Engineering and in the National Engineering Lab for Automotive Electronics and Control Technology, SJTU. His current research interests include power management strategies, power electronics devices and electric motor control systems for alternative-fuel vehicles.

Zhe Li received his B.E. degree in Mechanical Engineering and Automation from the Department of Mechanical Engineering, Zhengzhou University, Zhengzhou, China, in 2012. He is presently working towards his Ph.D. degree in Mechanical Engineering in the School of Mechanical Engineering, Shanghai Jiao Tong University, Shanghai, China. His current research interests include soft-switching power converters and inductive-based wireless power transfer systems.

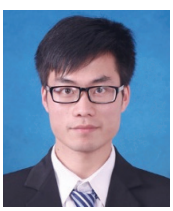

Wenqiang Jin received his B.S. degree in Mechanical Engineering from Shanghai Jiao Tong University, Shanghai, China, in 2017, where he is presently working towards his M.S. degree in Vehicle Engineering. Since August 2017, he has been working on project at the Argonne National Laboratory, Lemont, IL, USA. His current research interests include intelligent transportation systems, adaptive traffic signal control, traffic modeling and simulation, and connected vehicle technology.

Jochen Wiedemann received his B.S. degree from Ruhr University Bochum, Bochum, Germany, in 1977; and his M.S. and PhD degrees from the von Karman Institute for Fluid Dynamics, Sint-Genesius-Rode, Belgium, in 1978 and 1983, respectively. He worked at Ruhr University Bochum as a Research Assistant in the Institute of Thermo and Fluid Dynamics from 1977 to 1983. He joined the Department of Bodywork Technology and Aerodynamics at AUDI AG in 1984, where he became a Technical Specialist and a Member of the Extended Management Team in 1991, and a Management-Project Manager for the Audi Wind Tunnel Center in 1995. He has been working as a Professor at the University of Stuttgart, Stuttgart, Germany, as a Chair in the Department of Automotive Engineering, Institute of Internal Combustion Engines and Automotive Engineering, and as a Member of the Board of Directors of the FKFS-Research Institute of Automotive Engineering and Vehicle Engines since 1998. He was a Chairman of the Executive Board of FKFS from 1998 to 2000. He has been teaching Vehicle Aerodynamics at Tongji University, Shanghai, China, since 2002. He has been in charge of a number of research projects including a major DFG instrument program and cooperative projects with nearly all of the world-famous auto enterprises. His current research interests include automotive technology, aerodynamics, driving dynamics, transient aerodynamics, aerodynamics-driving, dynamics interactions, vehicle-driver interaction, acoustics and comfort (NVH), thermal management, etc.